Composite Structures 149 (2016) 125–133

Contents lists available at ScienceDirect

Composite Structures

journal homepage: www.elsevier.com/locate/compstruct

Flexural stiffness of thick walled composite tubes

M.I. Geuchy Ahmad, S.V. Hoa *

Concordia Center for Composites (CONCOM), Department of Mechanical and Industrial Engineering, Concordia University, Montreal, Quebec, Canada

ARTICLE INFO

Article history:
Received 26 February 2016
Accepted 28 March 2016
Available online 6 April 2016

Keywords:
Composite tubes
Flexural stiffness
Strength of materials
Elasticity
Experimental
Pure bending

ABSTRACT

Composite tubes have been used in many applications such as pipes, robot arms, drive shafts, electrical conduits, printing rollers, tube structures for sports equipment, rocket structures, satellite truss structures, landing gears for helicopters, and structural building members etc. For thin wall tubes made of isotropic materials, the flexural stiffness is usually determined by using strength of material approach with the expression *EI*, where *E* is the material modulus and *I* the cross section inertia. For composite tubes where many layers with different orientations are involved, the situation is more complex. Comparison of the results obtained using strength of materials equation and equation based on elasticity shows a large difference. In order to be sure of the validity of the results, experimental validation is necessary.

This paper presents the experimental work done on the determination of the flexural stiffness of thick composite tubes. Thick composite tubes were manufactured using an automated fiber placement machine. A special test set up was developed to subject the tubes to pure bending. Both strain gages and Digital Image Correlation were used to determine the strains, and subsequently the flexural stiffness. Experimental flexural stiffnesses of the tubes were determined. Results are compared with those calculated using the different equations.

1. Introduction

The case of a composite cylinder subjected to bending loading has received attention of many researchers. Several studies have applied the three-dimensional elasticity theories for analysis of composite cylinders under bending. Lekhnitskii [1] is known to be the first who used elasticity theory to solve the boundary value problem of a single layered anisotropic cylinder subjected to pure bending, and axisymmetric loading. Jolicoeur and Cardou [2] extended Lekhnitskii theory to obtain three-dimensional solutions of multilayered coaxial orthotropic straight cylinders under bending, torsion, and extension loads. Tarn and Wang [3] reformulated the governing equations of Lekhnitskii [1] to be decoupled into three sets of first order differential equations, allowing simpler formulation for multilayered anisotropic cylinders. Xia et al. [4] applied the classical lamination theory with Lekhnitskii's stress function approach [3] to study filament-wound fiber-reinforced sandwich pipes. Librescu and Song [5] derived a nonconventional beam theory based on first order plate theory for the analysis of composite beams of closed cross-section contour under general loading conditions. The theory was assumed to handle thin to thick-walled composite cylinders, by incorporating the effect of the three dimensional elastic effects and considering the transverse shear deformation. Kim and White [6] proposed a similar theory for analysis of thick hollow composite beams. Shadmehri et al. [7] used the approach of Librescu and Song [5] to derive equations to determine the flexural stiffness of thin composite tubes. There are many publications that used the finite element method for analysis of composite cylinders under bending. Bathe and Almeida [8] presented an effective beam element for analysis of both straight and curved composite tubes including cross section ovalization effects. Yan et al. [9] proposed an enhanced version of this element for elastic and non-linear plastic analysis of composite tubes. Qi and Jiang [10] presented a different beam element for analysis of straight and tapered composite tubes under general loading. Xu et al. [11] used a three dimensional solid element to model the four-point bending of a thermoplastic composite tubes until its ultimate failure. Derisi et al. [12–14] proposed a strain controlled method to develop thick composite tubes that exhibit large deformation. While the formulation of Jolicoeur and Cardou [2] can provide the solution for tubes, it is limited to lay up sequences of $[\theta/-\theta]$ only and the solution breaks down for layers with orientation of 0° and 90°. Zhang and Hoa provided solution for composite tubes made of [0/90] lay up sequence [15] and for the case of general lay up sequence including 0°, 90° and $[\theta/-\theta]$ in [16].

* Corresponding author.
E-mail address: hoasuon@alcor.concordia.ca (S.V. Hoa).

http://dx.doi.org/10.1016/j.compstruct.2016.03.050
0263-8223/

2. Different equations for the calculation of the flexural bending stiffness behavior

According to classical beam theory, the bending stiffness property describes the relation between an applied bending moment (M_z) and the obtained beam curvature (k) such that:

$$\langle EI\rangle = \frac{M_z}{k} \tag{1}$$

where EI is the bending stiffness of the beam. For a tube made of isotropic material, of circular cross-section, the bending stiffness is calculated using the following equation:

$$\langle EI\rangle = EI_T = E\frac{\pi}{64}(D_o^4 - D_i^4) \tag{2}$$

where, (E) is the extensional modulus of the isotropic material, (I_T) is the total area moment of inertia of the beam cross section, and (D_i), (D_o) are the tube inner, and outer diameters, respectively.

For composite tubes, the situation is more complicated. Composite structures are normally made of (N) number of layers having different orientation angles. The anisotropic nature of these layers causes the existence of different responses compared to isotropic ones. For example, the existence of shear-extension coupling produces an effect such that the normal stresses cause shear strains. Also, the layers interaction in composite structures leads to more complicated behavior. One may be tempted to use Eq. (2) by replacing the modulus E with the modulus E_x which takes into account the angle between the fiber and the axis of the tube. For tubes made of layers at angle of $\pm\theta$ with the tube axis, it is given by [18]:

$$E_x = \frac{E_1}{\cos^4\theta + \left(\frac{E_1}{G_{12}} - 2\nu_{12}\right)\cos^2\theta\sin^2\theta + \frac{E_1}{E_2}\sin^4\theta} \tag{3}$$

where:

E_1, E_2 --- extensional moduli in fiber and transverse directions of a layer, respectively.

G_{12}, ν_{12} --- Shear modulus and in-plane Poisson's ratio of a layer, respectively.

For the case of a single layer, Eq. (2) can then modified to be:

$$\langle EI\rangle_x = E_x I_T = E_x\frac{\pi}{64}(D_o^4 - D_i^4) \tag{4}$$

In case of multiple layers, Eq. (4) may be modified to be:

$$\langle EI\rangle_x = E_{x1}I_1 + E_{x2}I_2 + \cdots E_{xn}I_n \tag{5}$$

Eq. (5) does not take into account the interaction between layers of different angles. As such it may or may not be correct. Three dimensional elasticity may provide a better solution.

Based on the three dimensional theory of elasticity, Jolicoeur and Cardou [2] derived the following formula for calculating the bending stiffness of a composite tube.

$$\langle EI\rangle_{3D} = \sum_{n=1}^{N}\frac{\pi}{C_{33,n}}\left\{\begin{array}{l}\sum_{i=1}^{4}K_{i,n}[C_{34,n}*g_{i,n}*m_{i,n} - C_{13,n} - C_{23,n}(m_{i,n}+1)] \\ \quad\times\left[\frac{b_n^{(m_{i,n}+2)} - a_n^{(m_{i,n}+2)}}{(m_{i,n}+2)}\right] + \\ [1-\mu_{1,n}(C_{13,n}+3C_{23,n}) + 2\mu_{2,n}C_{34,n}]\left[\frac{b_n^4 - a_n^4}{4}\right]\end{array}\right\} \tag{6}$$

where:

- a_n, b_n --- Inner and outer radii of the composite layer, respectively
- $K_{i,n}$ --- Variables function of the layer orientation angle, the composite material properties, and inner and outer radii of the whole layers of the composite tube.

For the sake of clarity and completeness, some of the derivations of Jolicoeur and Cardou [2] are repeated here, to show how the terms of Eq. (6) are calculated.

The strain–stress relation for a layer can be written as:

$$\begin{bmatrix}\varepsilon_r\\ \varepsilon_\theta\\ \varepsilon_z\\ \gamma_{\theta z}\\ \gamma_{rz}\\ \gamma_{r\theta}\end{bmatrix} = \begin{bmatrix}C_{11} & C_{12} & C_{13} & C_{14} & 0 & 0\\ C_{12} & C_{22} & C_{23} & C_{24} & 0 & 0\\ C_{13} & C_{23} & C_{33} & C_{34} & 0 & 0\\ C_{14} & C_{24} & C_{34} & C_{44} & 0 & 0\\ 0 & 0 & 0 & 0 & C_{55} & C_{56}\\ 0 & 0 & 0 & 0 & C_{56} & C_{66}\end{bmatrix}\begin{bmatrix}\sigma_r\\ \sigma_\theta\\ \sigma_z\\ \tau_{\theta z}\\ \tau_{rz}\\ \tau_{r\theta}\end{bmatrix} \tag{7}$$

where r, θ, and z represent the radial, circumferential and axial direction, respectively.

Assume that each layer is an orthotropic material, in terms of the on-axis elastic constants, the coefficients of off-axis compliance C_{ij} can be expressed in terms of on –axis compliance coefficients as:

$$\begin{aligned}
C_{11} &= S_{33}\\
C_{12} &= S_{23}\cos^2\theta + S_{13}\sin^2\theta\\
C_{13} &= S_{13}\cos^2\theta + S_{23}\sin^2\theta\\
C_{14} &= 2(S_{13} - S_{23})\cos\theta\sin\theta\\
C_{22} &= S_{22}\cos^4\theta + (2S_{12} + S_{66})\cos^2\theta\sin^2\theta + S_{11}\sin^4\theta\\
C_{23} &= (S_{11} + S_{22} - S_{66})\cos^2\theta\sin^2\theta + S_{12}(\sin^4\theta + \cos^4\theta)\\
C_{24} &= (2S_{12} - 2S_{22} + S_{66})\cos^3\theta\sin\theta + (2S_{11} - 2S_{12} - S_{66})\cos\theta\sin^3\theta\\
C_{33} &= S_{11}\cos^4\theta + (2S_{12} + S_{66})\cos^2\theta\sin^2\theta + S_{22}\sin^4\theta\\
C_{34} &= (2S_{11} - 2S_{12} - S_{66})\cos^3\theta\sin\theta + (S_{66} + 2S_{12} - 2S_{22})\cos\theta\sin^3\theta\\
C_{44} &= S_{66}(\cos^2\theta - \sin^2\theta)^2 + 4(S_{11} + S_{22} - 2S_{12})\cos^2\theta\sin^2\theta\\
C_{55} &= S_{55}\cos^2\theta + S_{44}\sin^2\theta\\
C_{56} &= (S_{55} - S_{44})\cos\theta\sin\theta\\
C_{66} &= S_{44}\cos^2\theta + S_{55}\sin^2\theta
\end{aligned} \tag{8}$$

and where:

$$\begin{aligned}
S_{11} &= \frac{1}{E_1} \quad S_{12} = -\frac{\upsilon_{12}}{E_1} \quad S_{13} = -\frac{\upsilon_{13}}{E_1}\\
S_{22} &= \frac{1}{E_2} \quad S_{23} = -\frac{\upsilon_{23}}{E_2}\\
S_{33} &= \frac{1}{E_3}\\
S_{44} &= \frac{1}{G_{23}}\\
S_{55} &= \frac{1}{G_{13}}\\
S_{66} &= \frac{1}{G_{12}}
\end{aligned} \tag{9}$$

Notice that in Eq. (8), terms containing odd functions of $\sin\theta$ are C_{14}, C_{24}, C_{34}, and C_{56}. These terms will change sign when the layer angle changes from θ to $-\theta$.

Reduced elastic constants β_{ij} can be expressed in terms of the elastic constants C_{ij} as:

$$\beta_{ij} = C_{ij} - \frac{C_{i3}C_{3j}}{C_{33}} \tag{10}$$

with $\beta_{i3} = \beta_{3j} = 0$.

Notice that only terms β_{14}, β_{24}, β_{34}, and β_{56} will change sign as the fiber angle θ changes to $-\theta$.

After utilizing the stress–strain relations and stress functions, governing equations were derived. Using the method of separation

of variables, for the pure bending case, the stress functions are expressed as:

$$F = f_1(r)[k_x \sin\theta - k_y \cos\theta]$$
$$\varphi = \phi_1(r)[k_x \sin\theta - k_y \cos\theta] \tag{11}$$

where k is curvature in the plane perpendicular to direction i.

The solution for the governing equations has two parts: Homogeneous part and particular part. The total solution is:

$$f_1(r) = \sum_{i=1}^{4} \frac{K_i}{m_i} r^{m_i+1} + K_5 r + K_6 r \ln r + \frac{\mu_1}{2} r^3$$
$$\varphi_1 = \sum_{i=1}^{4} K_i g_i r^{m_i} + K_6 \frac{\beta_{56}}{\beta_{66}} + \mu_2 r^2 \tag{12}$$

where K_i are arbitrary constants, and

$$g_i = \frac{\beta_{24} m_i^2 + (\beta_{14} + \beta_{24}) m_i - \beta_{56}}{\beta_{44} m^2 - \beta_{55}} \tag{13}$$

and m_i are the roots of the characteristic equation:

$$a m^6 + b m^4 + c m^2 = 0 \tag{14}$$

where:

$$a = \beta_{22}\beta_{44} - \beta_{24}^2$$
$$b = \beta_{24}(2\beta_{14} + \beta_{24} + 2\beta_{56}) - \beta_{44}(\beta_{11} + 2\beta_{12} + \beta_{22} + \beta_{66}) - \beta_{22}\beta_{55} + \beta_{14}^2$$
$$c = \beta_{55}(\beta_{11} + 2\beta_{12} + \beta_{22} + \beta_{66}) - \beta_{56}^2 \tag{15}$$

Notice that as the fiber angle changes from θ to $-\theta$, the terms a, b, c do not change.

The characteristic equation has two double roots $m = 0$ and four roots given as:

$$m_{1..4} = \pm\sqrt{\frac{-b \pm \sqrt{b^2 - 4ac}}{2a}} \tag{16}$$

and

$$\begin{bmatrix} \mu_1 \\ \mu_2 \end{bmatrix} = \begin{bmatrix} -2\beta_{14} - 6\beta_{24} + \beta_{56} & 4\beta_{44} - \beta_{55} \\ -\beta_{11} - 2\beta_{12} + 3\beta_{22} - \beta_{66} & 2\beta_{14} - 2\beta_{24} + \beta_{56} \end{bmatrix}^{-1} \frac{1}{C_{33}} \begin{bmatrix} 2C_{34} \\ C_{13} - C_{23} \end{bmatrix} \tag{17}$$

or

$$\begin{bmatrix} \mu_1 \\ \mu_2 \end{bmatrix} = \frac{1}{BC - AD} \begin{bmatrix} -(2\beta_{14} - 2\beta_{24} + \beta_{56}) & 4\beta_{44} - \beta_{55} \\ -\beta_{11} - 2\beta_{12} + 3\beta_{22} - \beta_{66} & -(-2\beta_{14} - 6\beta_{24} + \beta_{56}) \end{bmatrix}^{-1} \times \frac{1}{C_{33}} \begin{bmatrix} 2C_{34} \\ C_{13} - C_{23} \end{bmatrix} \tag{18}$$

where:

$$A = -2\beta_{14} - 6\beta_{24} + \beta_{56}$$
$$B = 4\beta_{44} - \beta_{55}$$
$$C = -\beta_{11} - 2\beta_{12} + 3\beta_{22} - \beta_{66}$$
$$D = 2\beta_{14} - 2\beta_{24} + \beta_{56} \tag{19}$$

Notice that as the fiber angle θ changes sign, only the term μ_2 changes sign, while the sign of the term μ_1 stays the same. It can also be seen from Eqs. (16) and (13) that as the fiber angle θ changes sign, the terms m_i do not change sign, while the term g_i will change sign.

The constants K_i are determined using the continuity conditions at the interfaces between the layers.

For non slip condition at the interface e, these are:

For continuity of radial stress σ_r

$$\sum_{i=1}^{4} K_{i,n} e^{m_{i,n}-1} - K_{i,n+1} e^{m_{i,n+1}-1} = (\mu_{1,n+1} - \mu_{1,n}) e$$

For continuity of interlaminar stress τ_{rz}

$$\sum_{i=1}^{n} K_{i,n} g_{i,n} e^{m_{i,n}-1} - K_{i,n+1} g_{i,n+1} e^{m_{i,n+1}-1} = (\mu_{2,n+1} - \mu_{2,n}) e$$

For continuity of displacement u_r

$$\sum_{i=1}^{4} K_{i,n} U'_{i,n} e^{m_{i,n}} - K_{i,n+1} U'_{i,n+1} e^{m_{i,n+1}} = (U'_{5,n+1} - U'_{5,n}) e^2$$

For continuity of displacement u_θ

$$\sum_{i=1}^{4} K_{i,n} V'_{i,n} e^{m_{i,n}} - K_{i,n+1} V'_{i,n+1} e^{m_{i,n+1}} = (V'_{5,n+1} - V'_{5,n}) e^2$$

For continuity of displacement w

$$\sum_{i=1}^{4} K_{i,n} W'_{i,n} e^{m_{i,n}} - K_{i,n+1} W'_{i,n+1} e^{m_{i,n+1}} = (W'_{5,n+1} - W'_{5,n}) e^2 \tag{20}$$

where:

$$U'_i = \frac{1}{m_i}[\beta_{11} + \beta_{12}(m_i + 1) - \beta_{14} g_i m_i]$$
$$U'_5 = \frac{1}{2}\left[\mu_1(\beta_{11} + 3\beta_{12}) - 2\mu_2\beta_{14} + \frac{C_{13}}{C_{33}}\right]$$
$$V'_i = \frac{1}{m_i}[\beta_{11} + \beta_{12} - \beta_{22} m_i(m_i + 1) - g_i m_i(\beta_{14} - \beta_{24} m_i)]$$
$$V'_5 = \frac{1}{2}\left[\mu_1(\beta_{11} + \beta_{12} - 6\beta_{22}) - 2\mu_2(\beta_{14} - 2\beta_{24}) + \frac{C_{13} - 2C_{23}}{C_{33}}\right]$$
$$W'_i = \frac{1}{m_i}(\beta_{55} g_i - \beta_{56})$$
$$W'_5 = \frac{1}{2}(\beta_{55}\mu_2 - \beta_{56}\mu_1) \tag{21}$$

Also for the stress free condition at the inner (a) and outer (b) surfaces, we have (for radial stress = 0),

$$\sum_{i=1}^{4} K_{i,1} a^{m_{i,1}-1} = -\mu_{1,1} a$$

and

$$\sum_{i=1}^{4} K_{i,2} b^{m_{i,2}-1} = -\mu_{1,2} b \tag{22}$$

Notice that m_i and μ_1 do not change sign as the fiber angle changes from θ to $-\theta$, while g_i and μ_2 change sign.

For no friction at the interface e, instead of Eq. (20), we have Eq. (23) below:

$$\sum_{i=1}^{4} K_{i,n} e^{m_{i,n}-1} = -\mu_{1,n} e$$
$$\sum_{i=1}^{4} K_{i,n+1} e^{m_{i,n+1}-1} = -\mu_{1,n+1} e$$
$$\sum_{i=1}^{4} K_{i,n} g_{i,n} e^{m_{i,n}-1} = -\mu_{2,n} e$$
$$\sum_{i=1}^{4} K_{i,n+1} g_{i,n+1} e^{m_{i,n+1}-1} = -\mu_{2,n+1} e \tag{23}$$

Table 1
Material properties of carbon/epoxy used in bending stiffness analysis [18].

E_1, GPa	155
$E_2 = E_3$, GPa	12.1
$G_{12} = G_{13}$, GPa	4.4
G_{23}, GPa	3.2
$\nu_{12} = \nu_{13}$	0.248
ν_{23}	0.458

Eqs. (8), (13), (15), (16), (18), (20) or (23), and (22) provide information necessary for the evaluation of the $\langle EI\rangle_{3D}$ in Eq. (6).

In order to study the bending stiffness behavior of thick-walled composite tubes, a MATLAB program was written for these equations. The dimensionless parameter (t/D_o) is used to represent the wall thickness (t), fixing the tube outer diameter (D_o). The tube is considered to be thick when t/D_o is greater than 0.05 [17] and the maximum value of t/D_o equals to 0.5, at which the tube becomes a solid rod.

Using Eqs. (5) and (6), the bending stiffnesses are calculated, for thick-walled composite tubes made of $[\theta/-\theta]$ laminate configuration of equal layers thickness, and varying t/D_o from 0.05 to 0.45, using the properties of carbon/epoxy material, as listed in Table 1. Fig. 1 shows that there is a large difference between the value based on 3D elasticity (Eq. (6)) and that obtained using the strength of materials approach (Eq. (5)). The maximum difference is obtained at $\theta = 15°$ where the bending stiffness obtained by Eq. (6) is 2.5 times that obtained by Eq. (5). The difference lies mainly within the range of $0 < \theta < 50°$. At 0° and above 50°, the two equations give the same result.

Even though Eq. (6) was derived based on the more rigorous elasticity analysis, it is not absolutely certain that it is correct. Up to the present time, there has not been any experimental verification on the validity of this equation. As such, it is necessary to validate this equation using experimental results.

3. Experimental verification

In order to carry out the experiments to verify the results, there are a few requirements for the experiments in order to have meaningful comparison with experimental values. First the tubes need to be subjected to pure bending load, with minimum influence to the effect of local loading. Secondly the experiment should yield the flexural stiffness $\langle EI\rangle$ of the whole tube.

3.1. Pure bending test setup

The literature review shows the problems of using three-point bending and four-point bending tests for composite tubes [19,20], where the bending moment is introduced to the specimen by applying high concentrated transverse loads at the loading points. This way of loading causes high local deformation and premature failure for the test specimen under loading points. However the pure bending test setup is another different technique proposed in [21,22] for applying bending loading to the test specimen without applying any concentrated loading points. This technique was used for thin-walled composite cylinders of quite large diameters. In this section, the feasibility of this technique is checked for testing thick-walled composite tubes. This attempt is considered as the first time to test thick-walled composite tubes using the pure bending test setup.

The pure bending test setup in [22] has a loading capacity up to 1.5×10^6 lbf-in. (169 kN m) (Fig. 2). It is available at Concordia Center for Composites and was used for testing the tubes. The structural parts are rigid enough to prevent any deformation under the maximum loading. It can handle samples of different lengths from 30 to 48 in. (762–1219 mm). A schematic drawing for the pure bending test setup illustrates the main structural components is shown in Fig. 3.

The idea of the pure bending test rig is that the bending moment is introduced to the specimen in a smoother way compared to the conventional 3-point or 4-point bending tests. The test specimen ends are fixed inside the pure bending test rig using a low melting point alloy (LMPA). The hydraulic cylinders create the required loads which are converted to equal bending moments by rotating the moment-arm assemblies (moment-arm with the adaptor-plate and back-plate) about their pinions- (Fig. 3). This rotation generates shear forces between the LMPA and the surface of the tube ends such that the upper part of the sample is subjected to compression while the lower part is subjected to tension. These compression and tension forces form a moment at each end of the specimen without applying any concentrated load.

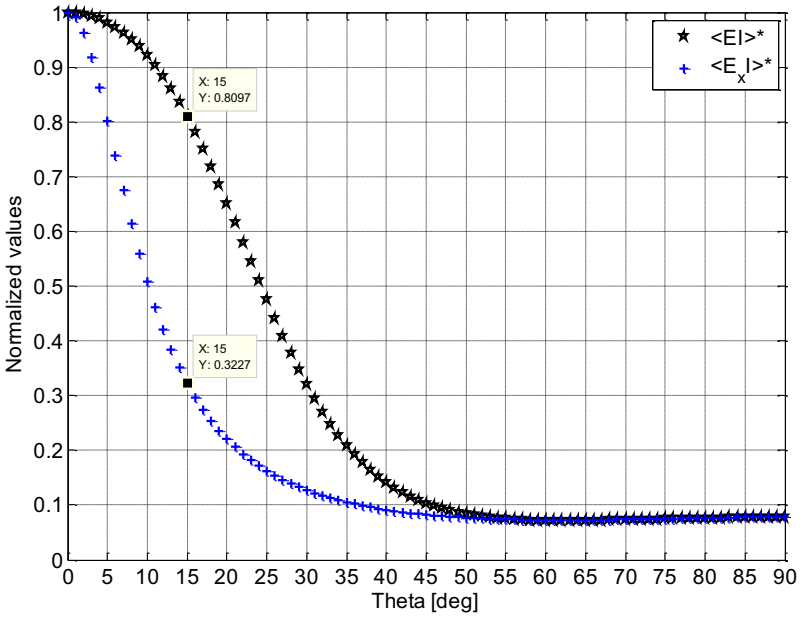

Fig. 1. Bending stiffness using Eq. (6) ($\langle EI\rangle$-upper curve)) and Eq. (5) (EI-lower curve) for tubes of $[\theta/-\theta]$, $t/D = 0.05$, $t/t = 0.5$. Values are normalized against $E_1 I_T$.

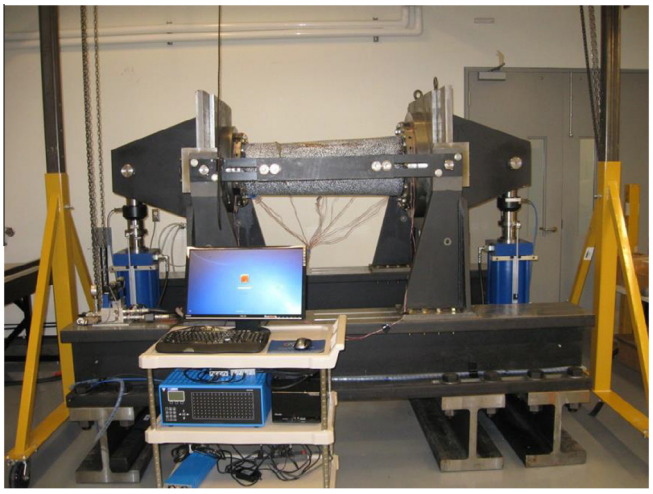

Fig. 2. Pure bending test setup designed at CONCOM [22].

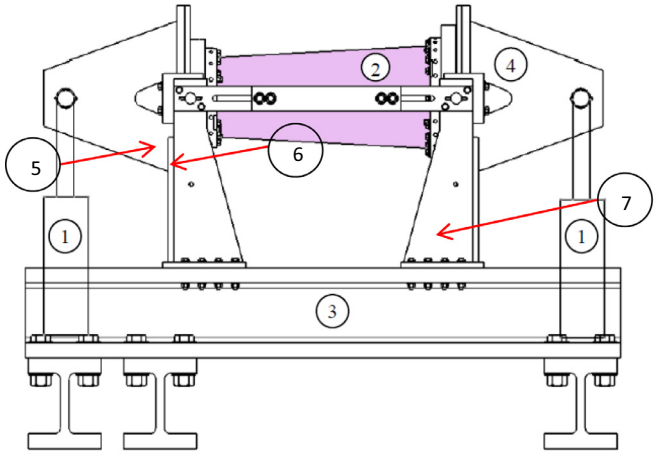

Fig. 3. Structural components of the pure bending test setup [22]. (1) Hydraulic cylinders, (2) Test specimen, (3) Reaction frame, (4) Moment-arm, (5) back-plate, (6) Adaptor-plate, (7) Pinion.

3.2. Determination of flexural bending stiffness from the pure bending tests

The bending stiffness of the tube can be obtained experimentally from the measured bending moment M_z and the end rotation angle of the tube (β) during the bending test. An accurate end rotation can be calculated using the following equation [21]

$$\beta(s) = \frac{L}{(D_o/2)}\varepsilon_z^{\max}(s) \tag{24}$$

where:

$\varepsilon_z^{max}(s)$ --- the axial strain at the mid length and mid circumference in the lower part of the tube ($\alpha = 270°$), corresponding to the bending moment M_z.

L --- half the length of the tube under pure bending ($L = 11$ inches "278.5 mm").

The tube curvature (k) is calculated from the following equation:

$$k(s) = \frac{\beta(s)}{L} \tag{25}$$

Substituting by Eq. (24) and (25) into Eq. (1), the bending stiffness equation will have the following form:

$$\langle EI \rangle = \frac{M_z(s)}{\varepsilon_z^{\max}(s)}\frac{D_o}{2} \tag{26}$$

Eq. (19) shows that the slope of ($M_z - \varepsilon_z^{max}$) curve is equal to the tube bending stiffness divided by the outer radius of the tube.

3.3. Tube designs

Fig. 1 shows that the largest difference between ⟨EI⟩ values calculated using the different equations occur within the range of angle $10° < \theta < 30°$. Tubes with $\theta = 25°$ were selected. This angle facilitates the fabrication process. In order to have reasonable thickness, tubes containing 90 layers (about 11.5 mm) were to be examined. Also two types of lay up sequence were examined. One was $[\theta/-\theta]_{45}$ and the other was $[\theta_{45}/-\theta_{45}]$. The interest was to see the effect of these stacking sequences on the flexural ending stiffness, and also on the strength of the tubes.

3.4. Tube fabrication

Two thick-walled tubes made of Carbon/PEEK thermoplastic composite material were manufactured. The material is supplied from TenCate Advanced Composites Company, having a commercial name "Cetex TC1200 PEEK AS-4", made of a semi-crystalline poly-ether-ether-ketone thermoplastic resin with unidirectional carbon fibers. The resin content is 34% by weight and 41% by volume. The first tube has a laminate configuration $[25_{45}/-25_{45}]$, meaning that the laminate is made of two thick layers; the inner layer is of orientation angle (25°) and the outer layer is of orientation angle (−25°). The second composite tube has a laminate configuration $[25/-25]_{45}$, which means the laminate consists of thin layers alternatively arranged. The tubes dimensions are: $D_o = 61.1$ mm (2.4 in.), $D_i = 38.1$ mm (1.5 in.), $t = 11.5$ mm (0.45 in.), $t/D_o = 0.19$. The tubes length is equal to 1016 mm (40 in.).

The thermoplastic composite tubes were manufactured using an automated fiber placement (AFP) machine, available at CONCOM (Fig. 4). The machine has 6 degrees of freedom. It can handle both thermoset composites and thermoplastic composites. For thermoplastic composites, it utilizes a hot gas torch that can melt a single tape 6.35 mm wide.

A mandrel is needed for the manufacturing process which should be stiff enough to withstand the applied compaction forces

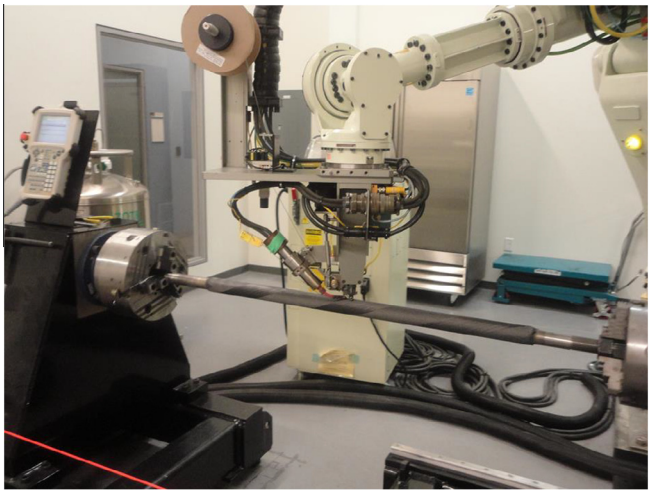

Fig. 4. Manufacturing of the thermoplastic composite tube using a robotic AFP machine.

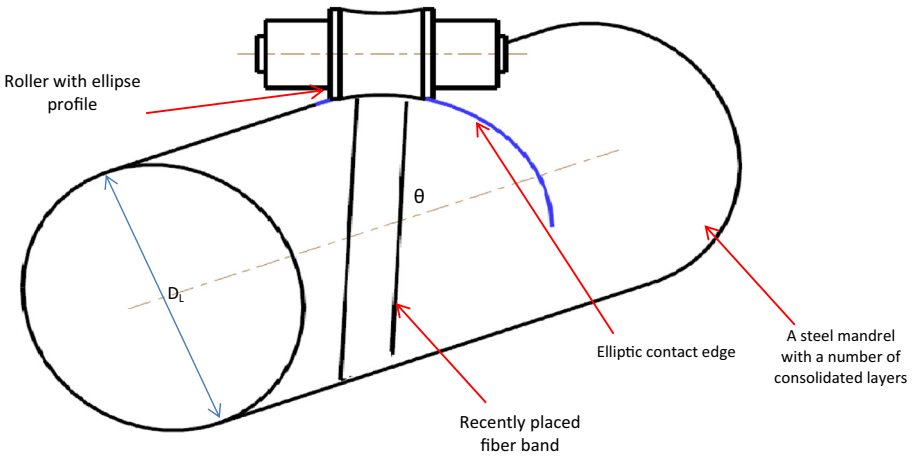

Fig. 5. Roller profile permits a maximum contact edge with the placed fiber band.

during the layup process and it should be extractable from the manufactured tube. A steel mandrel of diameter 1.5 in. is manufactured, polished and threaded at one end to be extracted easily after the manufacturing process. Steel rollers are designed and manufactured in order to be used in the layup process and to apply the compaction forces. The rollers have specific profiles to guarantee a maximum contact curve for the thermoplastic tape and the previous consolidated layers on the mandrel surface, (Fig. 5). The roller profile is generated by revolving an arc of an ellipse around the roller axis. The ellipse major diameter (D_x), and minor diameter (D_y) are specified according to the diameter of the placed layer (D_L) and its inclination angle (θ) as shown in Fig. 5, such that:

$$D_y = D_L$$
$$D_x = \frac{D_y}{\cos\theta} \tag{27}$$

Since D_L is increasing during the manufacturing process, four steel rollers are designed such that each roller is used for a specified range of D_L. The roller dimensions and their working range are tabulated in Table 2.

For the 90° layer, a roller with a straight cylinder is manufactured. All these rollers have a polished surface in order to have good surface finish for the manufactured part.

The manufacturing parameters for the tubes are listed in Table 3. For tube 1, the compaction force was 40 lbf and the hot gas temperature was 825 °C. Examination of a section of the material cut out from the tube shows significant amount of voids (Fig. 6).

Other process parameters were attempted on smaller samples to determine the optimal process conditions to provide tubes of better quality. These were used to fabricate tube 2. The process conditions for tube 2 are also shown in Table 3. In addition to the modification of the process parameters, a number of repasses were applied on top of the last layers. A repass is a pass without the deposition of materials. This means that the roller is run over

Table 2
Dimensions and the working range of the used compaction rollers.

Roller no	D [in]	D [in]	Diameter working range [in]
1	1.66	1.5	1.500–1.625
2	1.93	1.75	1.625–1.875
3	2.21	2	1.875–2.125
4	2.48	2.25	2.125–2.406

Table 3
Manufacturing parameters for the composite tubes.

	Tube 1 $[25_{45}/-25_{45}]$	Tube 2 $[25/-25]_{45}$
Compaction force (lbf)	40	75
HGT temperature (°C)	825	875
Nitrogen flow rate (L/min)	75	75
Laydown process rate inches/s (mm/s)	2.75 (70)	2.75 (70)
Number of compaction passes	0	2

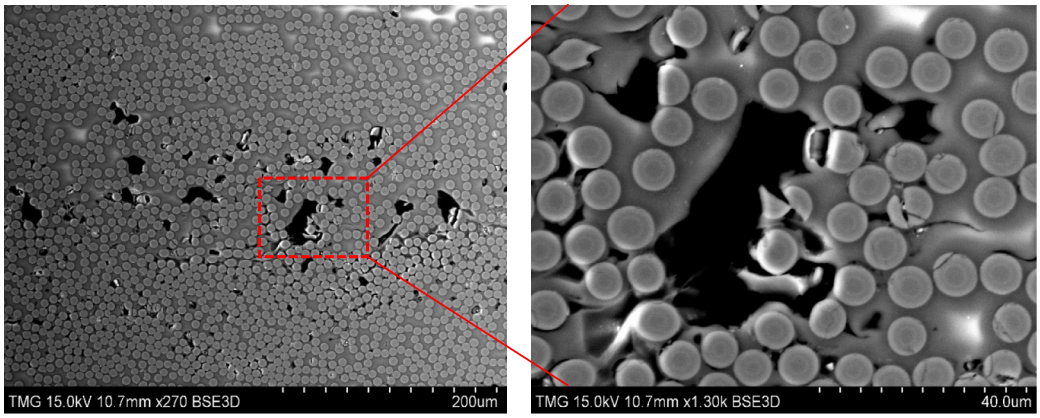

Fig. 6. Microscopic observation of a section of tube 1 shows significant amount of voids.

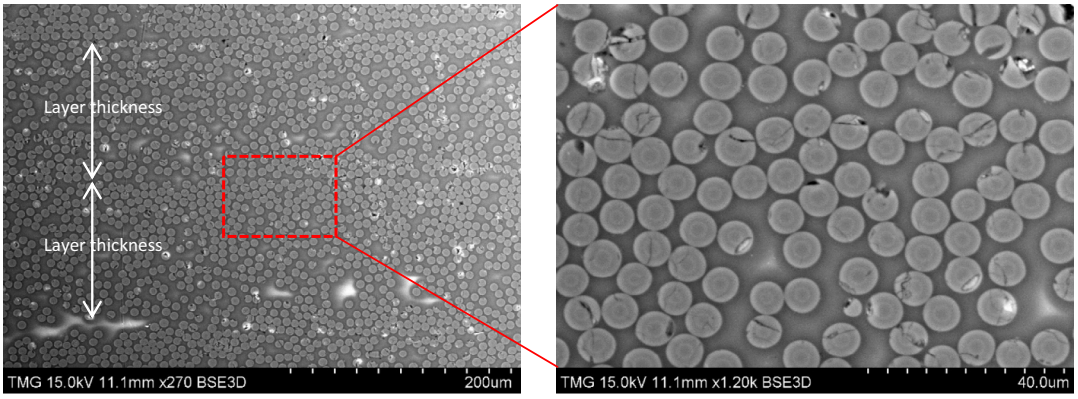

Fig. 7. Microscopic observation of a section of tube 2.

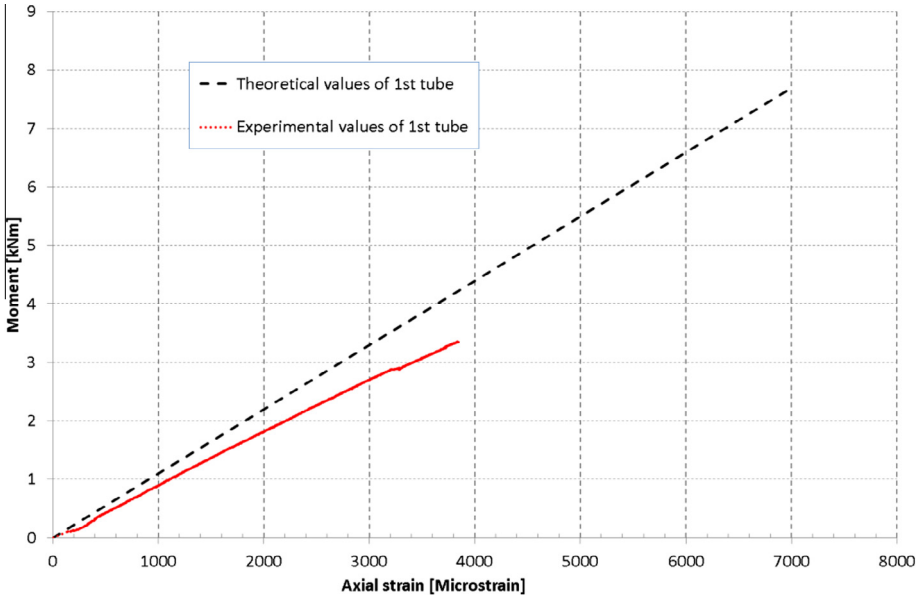

Fig. 8. Bending moment versus axial strain for tube 1.

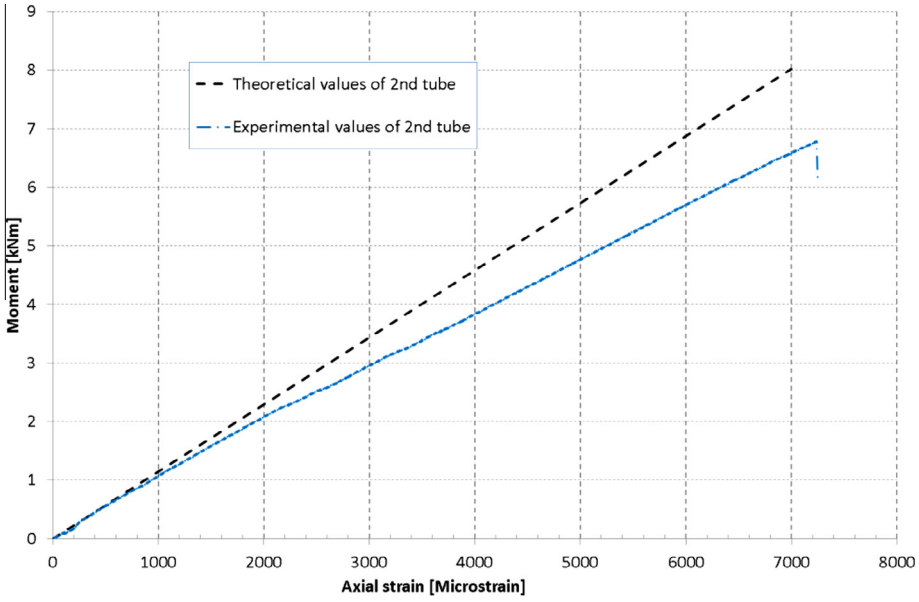

Fig. 9. Bending moment versus axial strain for tube 2.

Table 4
Material properties of Carbon/PEEK used in bending stiffness calculation [23,24].

	From ten cate [23]	Modified according to [24]
E_1, GPa	130	115
$E_2 = E_3$, GPa	10	10
$G_{12} = G_{13}$, GPa	5.2	5
G_{23}, GPa	5.2	5
$v_{23} = v_{13}$	0.33	0.329
v	–	0.49

the last deposited layer with the same pressure and temperature without adding new composite layer. This was found to help remove the voids, particularly on the last layers. Fig. 7 shows a micrograph of a section of tube 2. It can be seen that the quality is much improved.

4. Strain gaging and DIC

Strain gages were applied at different locations on the tubes, particular at the mid length, mid circumference at the bottom of the tube. In addition, speckle patterns were sprayed on the tube for Digital Image Correlation measurement.

5. Test results [25]

Fig. 8 shows the variation of the bending moment with respect to the axial strain at mid length-mid thickness at the bottom of tube 1 (continuous line). Also shown is a dotted line showing the theoretical calculated result. Fig. 9 shows the variation of the bending moment with respect to the axial strain at mid length-mid thickness at the bottom of tube 2 (continuous line). The dotted line shows the theoretical result. Note that the termination of the theoretical line does not indicate the theoretical strength, since this was not calculated.

The theoretical bending stiffness values were calculated using the properties of AS4/APC2 Carbon/PEEK thermoplastic composite, as obtained from TenCate [23] are listed in Table 4. It was assumed that these values were obtained from laminates made using autoclave. Modified properties according to [24] are also listed. The modification was done because it was found in [24] that when the thermoplastic material is in-situ consolidated using AFP, there is some difference with respect to those that are autoclave consolidated. The calculated bending stiffness is presented in Table 5.

Table 5
Results from bending of the tubes.

	$\langle EI \rangle$ Eq. (6) (kN m^2)	$\langle EI \rangle$ Eq. (5) (kN m^2)	$\langle EI \rangle$ Exp. (kN m^2)	Exp. Failure moments (kN m)
First tube	33.6	13.5	29.1	3.3
Second tube	35.0	13.5	32.3	6.78

The failure load of tube 1 is very low (3.3 kN m) as compared to that of tube 2 (6.78 kN m). Fig. 10 shows the mode of failure for tube 2. One can observe delamination and sliding of the outer most layers at the right side of the tube, fiber breakage at the failure zone in the layers below the outer layer, and local buckling for the delaminated fiber bands. Also one can see some location of matrix cracking on the outer layer. It is important to note that no failure occurred at the gripping zone at the tube ends which emphasizes the smooth introduction of the bending loading to the tube. Also no slipping occurred in the lower part of the tube at the gripping zones. This implies the effectiveness of the designed adaptor ring with the LMPA and the added tabs with the composite rings in preventing the slipping of the lower part of the tube under tension loading.

6. Discussion

6.1. Experimental flexural stiffness values

The experimental curves in Figs. 8 and 9 show an initial high slope followed by some decrease in slope. This is due to the ovalization effect when the tube is subjected to bending. Ovalization effect flattens the cross section of the tube and in turn decreases the stiffness. The equations shown earlier for the calculation of bending stiffness do not take ovalization effect into account. As such only the initial part of the curve was used for the determination of the flexural bending stiffness.

6.2. Comparison between theoretical values and experimental stiffness values

In terms of experimental values, tube 1 gives a stiffness of 29.1 kN m^2 while tube 2 gives a stiffness of 32.3 kN m^2. Eq. (5) (strength of materials) gives a value of 13.5 kN m^2 for both tubes while Eq. (6) (elasticity) gives a value of 33.6 kN m^2 for first tube

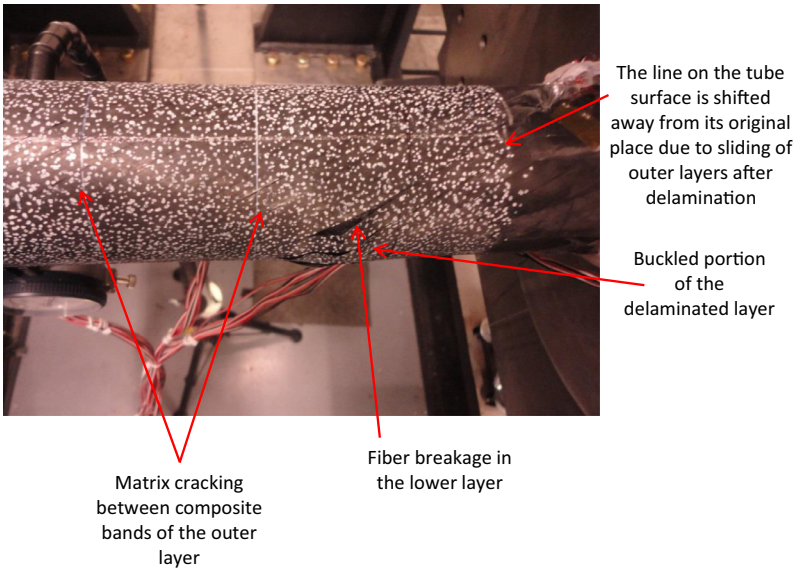

Fig. 10. Failure location of the second tube.

and 35 kN m^2 for tube 2. Thi gives more credibility to Eq. (6) since itself and experimental values for both tubes give similar results (within 10% of each other) while Eq. (5) is way off.

6.3. Effect of tube quality on bending stiffness

It is surprising to see that in spite of the presence of a significant amount of voids within its structure, tube 1 gives bending stiffness that is not too far off from the value of that of a good tube. This result was also observed from a previous work [22]. This does not mean that the tube with poor quality would have good strength (see below).

6.4. Effect of tube quality of its strength:

Tube 1 has very low strength (3.3 kN m) compared to tube 2 (6.78 kN m). The low strength can be due to two reasons. One is due to the lay up sequence where two blocks of layers of the same orientation are joined together at only interface [$25_{45}/-25_{45}$]. The other is the poor quality of the laminates due to the presence of voids.

7. Conclusion

The good agreement between the experimental and theoretical bending stiffness in both tubes gives confidence for the elasticity equation (6). Also both theoretical and experimental results show that the composite tube of larger number of sublaminates within the wall thickness has slightly higher bending stiffness, despite the two tubes have same dimensions, same number of layers, same orientation angle (−25/25), and made of the same thermoplastic composite material.

Acknowledgement

The financial support from the Natural Sciences and Engineering Research Council of Canada is appreciated.

References

[1] Lekhnitskii SG. Theory of elasticity of an anisotropic body. Moscow: Mir Publishers; 1981.
[2] Jolicoeur C, Cardou A. Analytical solution for bending of coaxial orthotropic cylinders. J Eng Mech 1994;120(12):2556–74.
[3] Tarn JQ, Wang YM. Laminated composite tubes under extension, torsion, bending, shearing and pressuring: a state space approach. Int J Solids Struct 2001;38:9053–75.
[4] Xia M, Takayanagi H, Kemmochi K. Bending behavior of filament-wound fiber-reinforced sandwich pipes. Compos Struct 2002;56(56):201–10.
[5] Librescu L, Song O. Free vibration of anisotropic composite thin-walled beams of closed cross-section contour. J Sound Vib 1993;V167(1):129–47.
[6] Kim C, White SR. Analysis of thick hollow composite beams under general loadings. Compos Struct 1996;34:263–77.
[7] Shadmehri F, Derisi B, Hoa SV. On bending stiffness of composite tubes. Compos Struct 2011;V(93).
[8] Bathe KJ, Almeida CA. A simple and effective pipe elbow element-linear analysis. J Appl Mech 1980;47(1):93–100.
[9] Yan AM, Jospin RJ, Nguyen DH. An enhanced pipe elbow element application in plastic limit analysis of pipe structures. Int J Numer Meth Eng 1999;46:409–31.
[10] Qi X, Jiang S. Design and analysis of a filament wound composite tube under general loadings with assistance of computer. In: 2nd international conference on education technology and computer (ICETC); 2010.
[11] Xu D, Derisi B, Hoa SV, Hojjati M, Fews R. Stress distributions of thermoplastic composite tubes subjected to four-point loading. In: The 1st joint Canadian–American international conference, Delaware, USA; 2009.
[12] Derisi B, Hoa SV, Hojjati M. Similitude study on bending stiffness behavior of composite tubes. J Compos Mater 2012;46(21):2695–710.
[13] Derisi B, Hoa SV, Xu D, Hojjati M, Fews R. Mechanical behavior of carbon/PEEK thermoplastic composite tube under bending load. J Thermoplast Compos Mater 2011;24(1):29–49.
[14] Derisi B, Hoa SV, Xu D, Hojjati M, Fews R. Composite tube exhibiting large deformation under bending. J Compos Mater 2010;44(16):2005–20.
[15] Zhang C, Hoa SV. A limit based approach to the stress analysis of cylindrically orthotropic composite cylinders (0/90) subjected to pure bending. Compos Struct 2012;94:2610–9.
[16] Zhang Canhui, Hoa Suong V, Liu Pei. A method to analyze the pure bending of tubes of cylindrically anisotropic layers with arbitrary angles including 0° and 90°. Compos Struct March 2014;109:57–67.
[17] Qatu MS, Sullivan RW, Wang W. Recent research advances on the dynamic analysis of composite shells: 2000–2009. Compos Struct 2010;93:14–31.
[18] Hyer M. Stress analysis of fiber-reinforced composite materials. Destech publications; 2009.
[19] Saga P. Experimental study of laminated composite tubes under bending [Master thesis]. University of Texas; 2007.
[20] Derisi B. evelopment of thermoplastic composite tubes for large deformation [Ph.D thesis]. Montreal, Quebec, Canada: Concordia University; 2008.
[21] Fuchs JP, Hyer MW, Starnes Jr., JH. Numerical and experimental investigation of the bending response of thin walled composite tubes. NASA-CR-195370, Blacksburg, Virginia; 1993.
[22] Shadmehri F. Buckling of laminated compoite conical shells: theory and experiment [Ph.D thesis]. Montreal, Quebec, Canada: Concordia University; 2012.
[23] TenCate Advanced Composites. enCate cetex thermoplastic advanced composites technical data; 2012.
[24] Leo JF, Hall JC, Kelly JJ, Bohlmann R. Design and testing of in situ consolidated thick high performance thermoplastics. In: Proc. 12th international conference on composite materials, Paris, France; 1999.
[25] El-Geuchy Ahmad MI. Bending behavior of thick walled composite tubes [Ph.D thesis]. Concordia University; 2013.